

Finite differences for coarse azimuthal discretization and for reduction of effective resolution near origin of cylindrical flow equations

Christophe Bogey*, Nicolas de Cacqueray, Christophe Bailly¹

Laboratoire de Mécanique des Fluides et d'Acoustique, UMR CNRS 5509, Ecole Centrale de Lyon, Université de Lyon, 69134 Ecully Cedex, France

ARTICLE INFO

Article history:

Received 9 December 2009

Received in revised form 18 October 2010

Accepted 24 October 2010

Available online 31 October 2010

Keywords:

Finite differences

Flow equations

Cylindrical coordinates

Azimuthal discretization

High-order

ABSTRACT

In this paper, the errors generated by the computation of derivatives in the azimuthal direction θ when flow equations are solved in cylindrical coordinates using finite differences are investigated. They might be large for coarse discretizations even using high-order schemes, which led us to design explicit finite differences specially for 8, 16, 32 and 64 points per circle. These schemes are shown to improve accuracy with respect to standard finite differences, and to provide solutions for a two-dimensional propagation problem similar to those obtained using Fourier spectral methods in the direction θ . A method is then presented to alleviate the time-step limitation resulting from explicit time integration near cylindrical origin, when finite differences are used. It consists in calculating azimuthal derivatives at coarser resolutions than permitted by the grid, in the same way as usually done using spectral methods. In practice, a series of doublings of the effective discretization in θ is implemented. Thus simulations can for instance be performed on a grid containing $n_\theta = 256$ points with a time step 32 times larger, with an accuracy comparable to that achieved in corresponding simulations involving Fourier spectral methods in the direction θ .

© 2010 Elsevier Inc. All rights reserved.

1. Introduction

The use of cylindrical or spherical coordinate systems is convenient to solve many physical configurations, including meteorological and geophysical problems, as well as basic fluid flows such as pipe flows and jets. It results however in specific issues which might decrease the accuracy or the computational efficiency of simulations if numerical methods are not appropriate. Spectral methods are for instance usually recommended for the computation of the derivatives in the azimuthal direction [1–3]. Compared to finite differences, these achieve high accuracy, but problems arising near the coordinate origin such as the singularity of the equations or the time-step limitation due to the clustering of points are still to be treated.

The special behaviour of flow equations at the origin of cylindrical coordinates has been considered in many studies. Procedures of different kind have been proposed. Among them, pole conditions serving as numerical boundary conditions have been constructed for pseudospectral schemes [4,5]. Methods based on series expansions of the variables around singularity have also been developed, and applied using finite differences [6,7]. In a different manner, the equations can be rewritten to obtain a form similar to that in Cartesian coordinates [8,9], thus simplifying the calculations at the coordinate origin. The coordinate singularity can also be avoided, by solving the flow equations in a Cartesian coordinate system at the origin [10], or by shifting the grid points in the radial direction by half the radial mesh spacing [11]. Another important problem

* Corresponding author. Address: Centre Acoustique, Ecole Centrale de Lyon, 36, Avenue Guy de Collongue, 69134 Ecully Cedex, France. Fax: 33 4 72 18 91 43.

E-mail addresses: christophe.bogey@ec-lyon.fr (C. Bogey), nicolas.cacqueray@ec-lyon.fr (N. de Cacqueray), christophe.bailly@ec-lyon.fr (C. Bailly).

¹ Institut Universitaire de France, France.

when using cylindrical coordinates is related to the very fine resolution near the singularity, which imposes a severe time-step restriction when time integration is explicit. This limitation can be alleviated by an appropriate rearrangement of the grid points to relieve the mesh density near the origin [12], or by the application of implicit differentiation schemes in the azimuthal direction [13,14]. When spectral methods are implemented in the azimuthal direction, it appeared also natural in many simulations [11,15–19] to reduce the effective resolution in the azimuth by artificially removing the highest Fourier modes. Finally, it can be noted that using finite-difference schemes for cylindrical coordinate system, energy conservation might not be strictly satisfied [20].

As mentioned above, it is usually most suitable, when using cylindrical coordinates, to employ spectral methods in the azimuthal direction because of their very high accuracy. Their computational costs might however be significant [3] for large numbers of points n_θ in the azimuth, reaching for example $n_\theta = 1024$ in recent works [21]. This may in particular be the case both for the Discrete Fourier Transform and for the Fast Fourier Transform algorithms whose costs are respectively proportional to n_θ^2 and to $n_\theta \times \log n_\theta$. Considering this, finite-difference schemes, which are relatively easy to implement, and whose cost increases linearly with n_θ , can be interesting to apply in the azimuthal direction. This has successfully been done by the authors over the last two years in large-eddy simulations of turbulent round jets [21–23] based on the three-dimensional cylindrical compressible Navier–Stokes equations. In these simulations, great care have been taken to minimize numerical errors and to preserve computational efficiency.

In the present paper, the accuracy obtained when flow equations are solved in cylindrical coordinates using finite differences is examined. The errors coming from the calculation of the derivatives in the azimuthal direction are first analyzed in the wave-number space, with the aim of showing that specific errors are generated in this case, and that they might be large even using high-order schemes. Explicit finite differences are therefore designed specially for azimuthal differentiation for 8, 16, 32 and 64 points per circle to remove these errors. Then the issue of the time-step limitation due to the fine mesh spacing near the cylindrical origin is addressed. Following a classical approach when spectral methods are used, a method is presented to reduce the effective resolution near the origin, allowing possible use of larger time steps when time integration is performed explicitly. It consists of changes in the implementation of finite differences in the azimuthal direction as the radial distance decreases. In addition, in order to illustrate and compare the algorithm properties, problems of acoustic propagation based on the polar Euler equations are solved using different methods in the azimuthal direction. The objective will be here to show that the solutions provided by the proposed schemes are more accurate than those calculated using standard finite differences for coarse discretizations, but also that they are similar to those obtained using Fourier spectral algorithms for azimuthal differentiation.

The paper is organized as follows. The Euler equations written in polar coordinates are first given in Section 2. The numerical artefacts generated by the discretization of the equations in the azimuthal direction using finite differences are characterized in Section 3. Differentiation schemes are then derived for coarse discretization. Section 4 is devoted to the approach of artificial reduction of the effective resolution near the coordinate origin. In both Sections 3 and 4, two-dimensional propagation problems are solved to assess the validity of the proposed algorithms with respect to standard high-order schemes and to Fourier spectral methods. Concluding remarks are finally drawn in Section 5.

2. Flow governing equations

The 2D Euler equations are expressed using the polar coordinates (r, θ) where r is the distance from the origin and θ is the azimuthal angle. They are written as:

$$\frac{\partial U}{\partial t} + \underbrace{\frac{1}{r} \frac{\partial r E}{\partial r} + \frac{1}{r} \frac{\partial F}{\partial \theta}}_{=H} + \frac{B}{r} = 0, \tag{1}$$

$$\text{where } U = \begin{bmatrix} \rho \\ \rho u_r \\ \rho u_\theta \\ \rho e \end{bmatrix}, \quad E = \begin{bmatrix} \rho u_r \\ \rho u_r^2 + p \\ \rho u_r u_\theta \\ (\rho e + p) u_r \end{bmatrix}, \quad F = \begin{bmatrix} \rho u_\theta \\ \rho u_r u_\theta \\ \rho u_\theta^2 + p \\ (\rho e + p) u_\theta \end{bmatrix}, \quad \text{and } B = \begin{bmatrix} 0 \\ -(\rho u_\theta^2 + p) \\ \rho u_r u_\theta \\ 0 \end{bmatrix}.$$

The variables ρ , u_r , u_θ and p denote density, radial and azimuthal velocities, and pressure. The total energy is given by $\rho e = p/(\gamma - 1) + \rho(u_r^2 + u_\theta^2)/2$ with $\gamma = 1.4$.

3. Finite-differences for coarse azimuthal discretization

3.1. Analysis of numerical error

For coarse azimuthal discretization, significant errors might be generated by the spatial derivatives in Eq. (1). Consider for instance a steady uniform flow field of velocity $\mathbf{u} = u\mathbf{x}$, where $\mathbf{x} = (x, y)$ are the Cartesian coordinates and u is a constant, theoretically verifying $\partial U/\partial t = H = 0$. Using polar coordinates, the velocity field is written as $u_r = u \cos \theta$ and $u_\theta = -u \sin \theta$, and vectors E , F and B become:

$$E = \begin{bmatrix} \rho u \cos \theta \\ \rho u^2 (\cos 2\theta + 1)/2 + p \\ -\rho u^2 \sin 2\theta/2 \\ (\gamma p/(\gamma - 1) + \rho u^2/2)u \cos \theta \end{bmatrix}, \quad F = \begin{bmatrix} -\rho u \sin \theta \\ -\rho u^2 \sin 2\theta/2 \\ \rho u^2 (1 - \cos 2\theta)/2 + p \\ -(\gamma p/(\gamma - 1) + \rho u^2/2)u \sin \theta \end{bmatrix} \quad \text{and} \quad B = \begin{bmatrix} 0 \\ -(\rho u^2 (1 - \cos 2\theta)/2 + p) \\ -\rho u^2 \sin 2\theta/2 \\ 0 \end{bmatrix}$$

Vectors E , F and B in Eq. (1) thus depend only on azimuthal angle θ , containing terms in $\sin\theta$, $\cos\theta$, $\sin 2\theta$ and $\cos 2\theta$.

For exact differentiation operators $\partial/\partial r$ and $\partial/\partial\theta$, it can be directly checked that:

$$H = \frac{1}{r} \frac{\partial rE}{\partial r} + \frac{1}{r} \frac{\partial F}{\partial\theta} + \frac{B}{r} = 0,$$

yielding $\partial U/\partial t = 0$ as expected for the considered steady and uniform flow field. However, using approximate derivatives $\partial^*/\partial r$ and $\partial^*/\partial\theta$, this might not be the case. The term

$$H^* = \frac{1}{r} \frac{\partial^* rE}{\partial r} + \frac{1}{r} \frac{\partial^* F}{\partial\theta} + \frac{B}{r} \neq 0, \tag{2}$$

has then to be evaluated to determine the errors generated by the differentiations.

This term is examined when explicit centered $(2n + 1)$ -point finite-difference schemes with coefficients a_j are used. For a polar grid with constant mesh spacings Δr and $\Delta\theta$ in the radial and azimuthal directions, one gets:

$$\frac{1}{r} \frac{\partial^* rE}{\partial r} = \frac{1}{r\Delta r} \sum_{j=-n}^n a_j (r + j\Delta r) E(r + j\Delta r) = \frac{E}{r}, \tag{3}$$

because vector E is only a function of the azimuth θ , and $\sum_{j=-n}^n a_j = 0$ and $\sum_{j=-n}^n j a_j = 1$ for centered finite differences, by construction. In the same way, one obtains :

$$\frac{1}{r} \frac{\partial^* F}{\partial\theta} = \frac{1}{r\Delta\theta} \sum_{j=-n}^n a_j F(\theta + j\Delta\theta). \tag{4}$$

Finite differences thus provide exact approximations of the derivatives in the radial direction, which is not the case in the azimuthal direction. Expressions (3) and (4) are then introduced in term (2) to calculate H^* . The first component of H^* , associated with the mass conservation equation, writes as:

$$H^*|_1 = \frac{\rho u}{r} \left[\cos \theta - \frac{\partial^* \sin \theta}{\partial\theta} \right] = \frac{\rho u}{r} \left[\cos \theta - \frac{1}{\Delta\theta} \sum_{j=-n}^n a_j \sin(\theta + j\Delta\theta) \right] = \frac{\rho u}{r} \cos \theta \left[1 - \frac{2}{\Delta\theta} \sum_{j=1}^n a_j \sin(j\Delta\theta) \right].$$

The error resulting from the azimuthal differentiation is given here by the function:

$$\mathcal{E}_{pol}^1(\Delta\theta) = 1 - \frac{2}{\Delta\theta} \sum_{j=1}^n a_j \sin(j\Delta\theta).$$

The same error function can be derived for the fourth component of H^* , related to the energy equation. For the second and third components of H^* , associated with the momentum conservation equations, it is found that:

$$H^*|_{2,3} = \frac{\rho u^2}{r} \begin{bmatrix} \cos 2\theta - \frac{1}{2} \frac{\partial^* \sin 2\theta}{\partial\theta} \\ -\left(\sin 2\theta - \frac{1}{2} \frac{\partial^* \cos 2\theta}{\partial\theta} \right) \end{bmatrix} = \frac{\rho u^2}{r} \begin{bmatrix} \cos 2\theta \left(1 - \frac{1}{\Delta\theta} \sum_{j=1}^n a_j \sin(2j\Delta\theta) \right) \\ -\sin 2\theta \left(1 - \frac{1}{\Delta\theta} \sum_{j=1}^n a_j \sin(2j\Delta\theta) \right) \end{bmatrix}.$$

In this case the numerical error is governed by the function

$$\mathcal{E}_{pol}^2(\Delta\theta) = 1 - \frac{1}{\Delta\theta} \sum_{j=1}^n a_j \sin(2j\Delta\theta),$$

which is also $\mathcal{E}_{pol}^2(\Delta\theta) = \mathcal{E}_{pol}^1(2\Delta\theta)$. The errors \mathcal{E}_{pol}^1 and \mathcal{E}_{pol}^2 coming from the approximate derivatives in the direction θ naturally depend on the finite-difference scheme applied, and on the azimuthal discretization, which can be characterized for an equally-spaced grid by the number of points per circle, hereafter denoted by PPC, defined by $PPC = 2\pi/\Delta\theta$. The variations of \mathcal{E}_{pol}^1 and \mathcal{E}_{pol}^2 when different explicit centered finite differences and discretizations are used, are illustrated in Figs. 1 and 2.

In Fig. 1, the azimuthal discretization errors are determined using standard differentiation schemes which are of order $2n$ for $(2n + 1)$ stencils, for grids with $PPC = 8, 16, 32$ and 64 . They are represented as functions of the stencil size, from $(2n + 1) = 3$ to 15 , yielding schemes of order 2 to 14. Using these schemes, whatever the grid discretization may be, the error \mathcal{E}_{pol}^2 resulting from the approximate derivatives of $\cos 2\theta$ and $\sin 2\theta$ is seen to be significantly higher than the error \mathcal{E}_{pol}^1 coming from the derivative of $\sin\theta$. Both errors however decrease rapidly with the scheme order, \mathcal{E}_{pol}^1 varying for instance, for 16

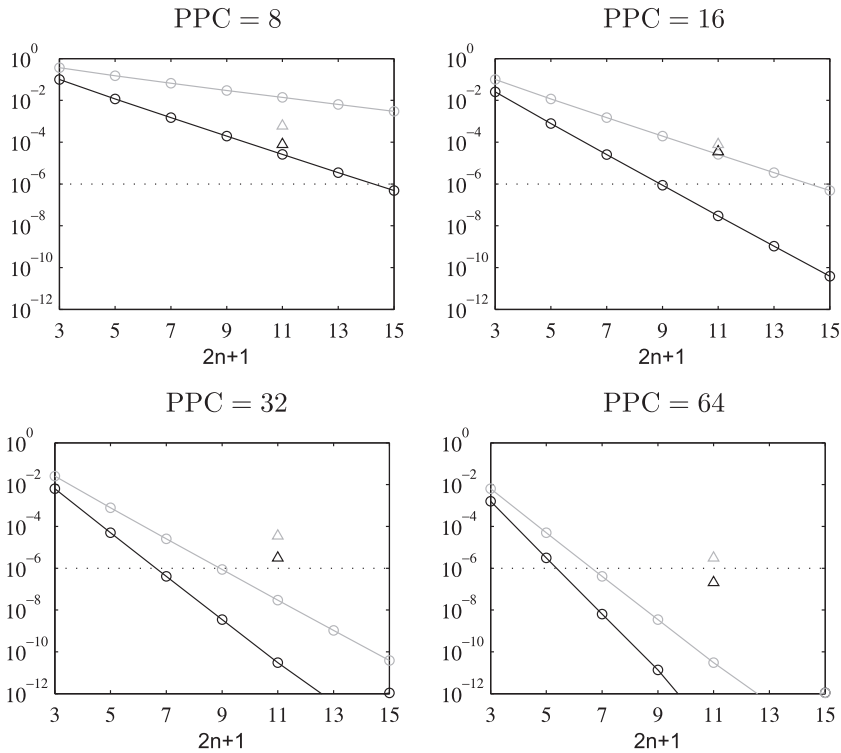


Fig. 1. Errors \mathcal{E}_{pol}^1 (in black), and \mathcal{E}_{pol}^2 (in gray), obtained for $PPC = 8, 16, 32$ and 64 using centered $(2n + 1)$ -point finite differences: \circ standard schemes of order $2n$, \triangle a 4th-order 11-point low-dispersion scheme [24]. The dotted line represents an error of 10^{-6} .

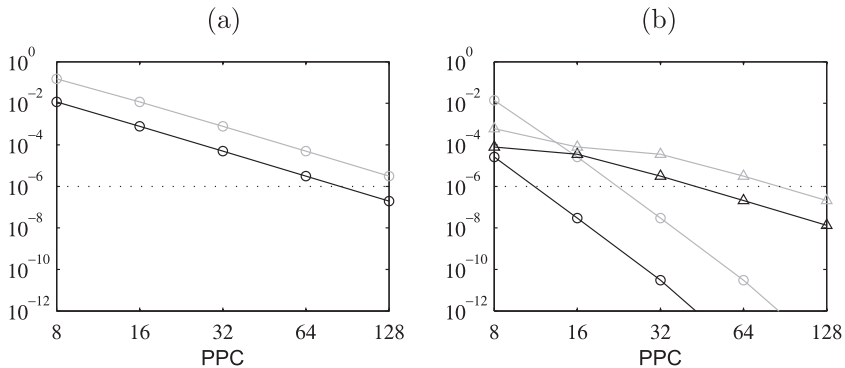


Fig. 2. Errors \mathcal{E}_{pol}^1 (in black), and \mathcal{E}_{pol}^2 (in gray), for an azimuthal discretization varying from $PPC = 4$ to $PPC = 128$, using: (a) \circ 4th-order 5-point finite differences; (b) \circ 10th-order 11-point finite differences, and \triangle a 4th-order 11-point low-dispersion scheme [24]. The dotted line represents an error of 10^{-6} .

points per circle, from about 10^{-2} using a 2nd-order scheme down to 10^{-10} using a 14th-order scheme. Schemes with increasing order must therefore be used to reduce the azimuthal differentiation errors. With fewer grid points in the azimuthal direction, schemes of higher-order must also be chosen to reach a given accuracy. To get \mathcal{E}_{pol}^2 lower than 10^{-6} for example, orders 6, 8 and 14 are respectively required for 64, 32 and 16 points per circle, whereas for 8 points per circle an order much higher than 14 is necessary.

For comparison, the errors obtained using a 4th-order 11-point scheme [24] designed to minimize dispersion down to four points per wavelength are also shown in Fig. 1 for the four azimuthal discretizations. Compared to the errors determined for the 10th-order scheme of same stencil size, they are smaller for $PPC = 8$, similar for $PPC = 16$, but appreciably higher for $PPC = 32$ and 64 . Thus using low-dispersion schemes instead of standard high-order schemes might increase the numerical errors generated by the azimuthal derivatives.

The reduction of the errors \mathcal{E}_{pol}^1 and \mathcal{E}_{pol}^2 with the number of points per circle is displayed in Fig. 2 for standard 4th- and 10th-order schemes and for the 11-point low-dispersion schemes considered above. As expected the decrease of the errors is

more rapid at order 10 than at order 4. It is however striking to notice that using the 4th-order scheme, $\mathcal{E}_{pol}^2 < 10^{-6}$ is not satisfied even for PPC = 128.

As for the use of the low-dispersion scheme instead of the standard scheme with the same stencil size, it leads to lower errors for PPC = 8, that is for a very coarse grid, but higher errors for finer azimuthal discretizations. To ensure $\mathcal{E}_{pol}^2 < 10^{-6}$ for example, 128 points are to be specified in the azimuth using the low-dispersion scheme, but only 32 points using the 10th-order scheme. The implementation of a low-dispersion scheme therefore appears appropriate only for very high PPC.

3.2. Development of specific schemes for azimuthal differentiation

To remove the azimuthal differentiation errors described above, which might be non negligible for coarse grids even using finite differences of very high-order, explicit 2nd-order centered finite differences are developed for 8, 16, 32 and 64 points per circle. For PPC = 8 and 16, schemes based on 7-point stencils, referred respectively to as FD8ppc and FD16ppc in Table 1, are proposed. Their coefficients a_j ($a_0 = 0$ and $a_{-j} = -a_j$) are determined so that:

$$\begin{cases} \sum_{-n}^n ja_j = 1, \\ \mathcal{E}_{pol}^1 = 0, \\ \mathcal{E}_{pol}^2 = 0. \end{cases} \tag{5}$$

The numerical errors generated for an uniform velocity field by the approximate derivatives of $\sin\theta$, $\sin2\theta$ and $\cos2\theta$ are thus nil.

For PPC = 32 and 64, 9-point finite differences, FD32ppc and FD64ppc, are designed. Their coefficients a_j , provided in Table 1, satisfy conditions (5) as previously. They are also chosen so that the phase error $|k^* - k|\Delta x/\pi$, where k^* is the wave number computed by the finite differences for the wave number k for a Δx grid spacing [25], given by:

$$k^* \Delta x = 2 \sum_{j=1}^n a_j \sin(jk\Delta x), \tag{6}$$

is lower than 5×10^{-4} over the largest wave-number range.

To check the properties of the schemes in the Fourier space, the effective wave numbers $k^*\Delta x$ and the phase errors $|k^* - k|\Delta x/\pi$ obtained for FD8ppc, FD16ppc, FD32ppc and FD64ppc are represented in Fig. 3 as functions of $k\Delta x$. As expected, the schemes built up to remove the derivation errors of $\sin\theta$, $\sin2\theta$ and $\cos2\theta$ for m points per circle generate no phase error for m and $m/2$ points per wave length. For FD8ppc developed for 8 points per circle for instance, the phase error is nil for $k\Delta x = \pi/4$ and $\pi/8$, corresponding to discretizations of 8 and 4 points per wave length.

Table 1
Coefficients of the finite differences for azimuthal discretizations of PPC = 8, 16, 32 and 64, with $a_0 = 0$ and $a_{-j} = -a_j$.

	FD8ppc	FD16ppc	FD32ppc	FD64ppc
a_1	0.819475776996	0.764510305787	0.827728256913	0.825858420492
a_2	-0.210854308895	-0.161835782187	-0.228094785916	-0.225946472928
a_3	0.034077613598	0.019720419529	0.050400938205	0.049278244240
a_4	0	0	-0.005685374924	-0.005450051839

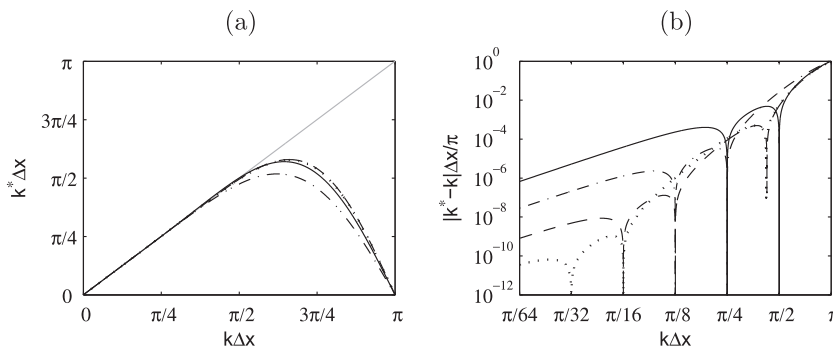


Fig. 3. Representation (a) of effective wave numbers $k^*\Delta x$ in linear scales, and (b) of phase errors $|k^* - k|\Delta x/\pi$ in logarithmic scales, as functions of the exact wavenumber $k\Delta x$, obtained for the schemes: — FD8ppc, - - - FD16ppc, - - - FD32ppc, ····· FD64ppc.

3.3. Application to the propagation of an acoustic pulse

To illustrate the accuracy of the schemes proposed, a two-dimensional test case is solved using polar Eq. (1). In the same way as in the first workshop on Computational Aeroacoustics [26], the propagation of a Gaussian acoustic pulse is considered. The initial acoustic pulse is placed in an uniform flow $u = Mx$, where $x = (x, y)$ are the Cartesian coordinates, with constant mean density and pressure. More precisely the conditions at $t = 0$ are:

$$\begin{aligned}
 p &= 1/\gamma + \mathcal{A} \exp[-(\ln 2)(x^2 + y^2)/b^2], \\
 \rho &= 1 + \mathcal{A} \exp[-(\ln 2)(x^2 + y^2)/b^2], \\
 u_x &= M, \\
 u_y &= 0,
 \end{aligned}
 \tag{7}$$

where $\mathcal{A} = 10^{-4}$ and $b = 6$ are respectively the magnitude and the half-width of the Gaussian pulse, which is initially located at $x = -15$ and $y = 0$ on the left-hand side of the origin $0 = (0, 0)$ of the polar coordinates. The mean flow velocity is $M = 0.5$. The acoustic wave generated by the pulse reaches the origin at time $t = 10$.

Polar Euler Eq. (1) are solved up to time $t = 20$ on uniform grids containing $n_r = 81$ points in the radial direction, and $n_\theta = \text{PPC} = 8, 16, 32$ or 64 points in the azimuthal direction. The mesh spacings are $\Delta r = 1$ and $\Delta\theta = 2\pi/\text{PPC}$, and the time step is $\Delta t = \text{CFL} \Delta r \Delta\theta / (1 + M)$ with $\text{CFL} = 5/(2\pi) \simeq 0.8$. Thus the number of time steps is 48 for $\text{PPC} = 8$, 96 for $\text{PPC} = 16$, 192 for $\text{PPC} = 32$, and 384 for $\text{PPC} = 64$. The method of Mohseni & Colonius [11] consisting in placing the first points in the radial direction at $r = \Delta r/2$ is implemented to avoid the treatment of the axis singularity. To focus on the errors generated by the azimuthal differentiation, the derivatives in the radial direction are calculated using 14th-order finite differences, whereas those in the azimuth are computed using standard finite differences, or the FD8ppc, FD16ppc, FD32ppc and FD64ppc schemes depending on the discretization, or spectral methods based on discrete Fourier transforms [16]. Time integration is performed using a low-storage 2nd-order 6-stage Runge–Kutta algorithm [24]. As required using centered finite-difference schemes [24,27–30], the flow variables are filtered explicitly at every time step by the application of a 14th-order filter sequentially in the radial and azimuthal directions with a strength of 0.5 for $\text{PPC} = 8$ and of 0.2 for $\text{PPC} = 16, 32$ and 64, a filtering strength of unity leading to a complete removal of grid-to-grid oscillations as defined in previous papers [24,30]). Finally the radiation conditions of Tam & Dong [31] are imposed at the boundaries using optimized explicit non-centered finite differences [32].

To characterize the accuracy of the numerical methods, the solutions are compared with the analytical solution of this initial value problem [25] given by:

$$p_{sol}(\mathbf{x}, t) = \frac{1}{\gamma} + \frac{\mathcal{A}}{2\alpha} \int_0^\infty \xi \exp[-\xi^2/4\alpha] \cos(t\xi) J_0(\xi\eta) d\xi,
 \tag{8}$$

where $\eta = \sqrt{(x - Mt)^2 + y^2}$, $\alpha = (\ln 2)/b^2$ and $J_0(z)$ is the Bessel function of first kind and order 0. The error rate with respect to the analytical solution is then

$$\mathcal{E}_{sol}(t) = \frac{[\int \int_S (p(t) - p_{sol}(t))^2 dS]^{1/2}}{[\int \int_S (p(t=0) - 1/\gamma)^2 dS]^{1/2}}.
 \tag{9}$$

The pressure fields obtained at $t = 20$ for 8 grid points per circle using 14th-order finite differences, the FD8ppc scheme and Fourier spectral methods in the azimuthal direction are shown in Fig. 4(a,b,c). They are compared to the exact pressure field represented in Fig. 4(d), which does not appear axisymmetric because of the very low grid resolution. The solution calculated using the 14th-order scheme strongly differs from the analytical solution, whereas the two other solutions roughly agree,

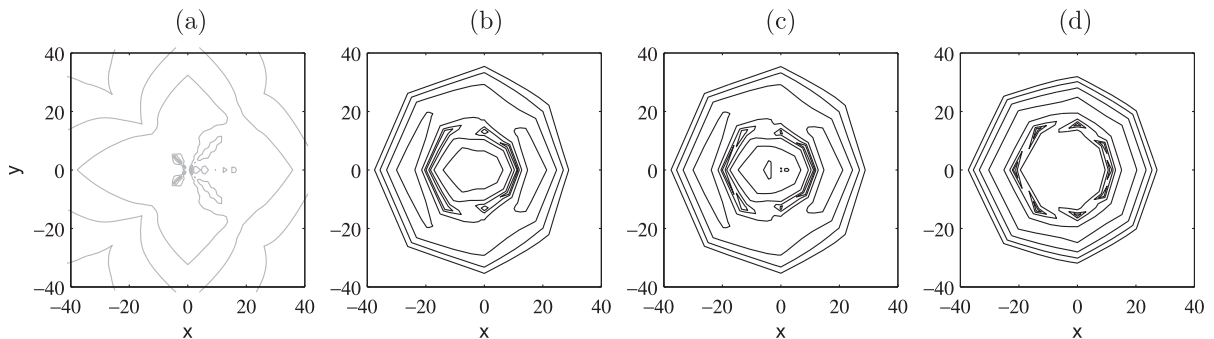


Fig. 4. Solutions obtained at $t = 20$ for $\text{PPC} = 8$, using (a) 14th-order finite differences, (b) the FD8ppc scheme, and (c) Fourier spectral method for azimuthal derivatives; (d) analytical solution. The contours of fluctuating pressure in black are for levels of $[1.75, 3.5, 7, 14] \times 10^{-6}$, those in grey are for $[50, 100, 200] \times 10^{-6}$.

both exhibiting a fair circular-wave-front shape. In the present case, the FD8ppc scheme is therefore much more accurate than the 14th-order scheme, which is remarkable given their respective 7-point and 15-point stencils. Its use also provides results similar to those determined when Fourier spectral methods are applied to the azimuthal differentiation.

The pressure fields obtained at $t = 20$ for $PPC = 16$ using 10th-order finite differences, the FD16ppc scheme and Fourier spectral methods in the azimuthal direction are now presented in Fig. 5(a,b,c). The solution calculated using the 7-point FD16ppc scheme is found to be in better agreement with the analytical solution in Fig. 5(d) than that computed using the 11-point 10th-order scheme. As previously, it also corresponds well to the solution provided by the simulation using Fourier spectral methods.

Pressure fields are not shown for $PPC = 32$ and $PPC = 64$, because they all look nearly alike. Instead, time variations of errors \mathcal{E}_{sol} with respect to the analytical solution are plotted in Fig. 6 for grid discretizations $PPC = 8, 16, 32,$ and 64 . The errors are evaluated from the solutions computed using 8th-order finite differences, the schemes proposed in the paper, and Fourier spectral methods for the azimuthal differentiation. Compared to those obtained for the 8th-order scheme in Fig. 6(a), the errors estimated for the proposed schemes in Fig. 6(b) are spectacularly lowered for the two coarser grids, they are slightly reduced for 32 points per circle, and they are similar for 64 points per circle. Moreover they do not differ appreciably from those reported in Fig. 6(c), whatever the resolution may be. This indicates that applying the proposed schemes rather than Fourier spectral methods does not lead here to a loss of accuracy.

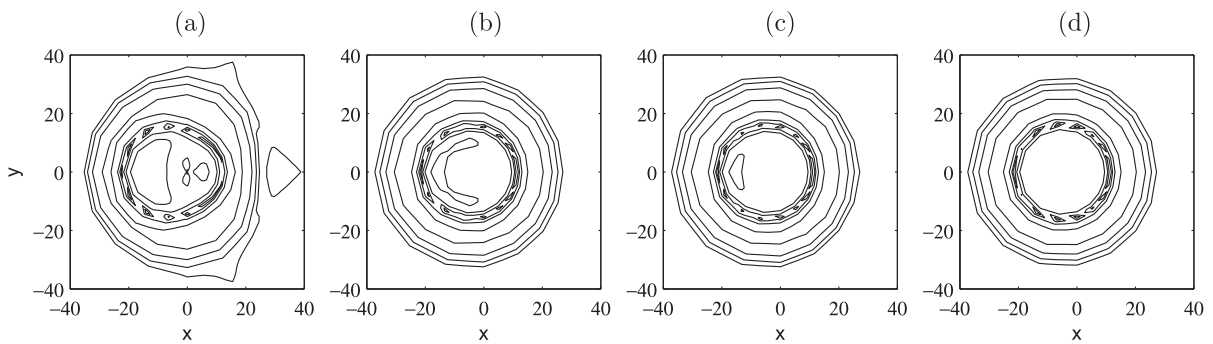


Fig. 5. Solutions obtained at $t = 20$ for $PPC = 16$, using (a) 10th-order finite differences, (b) the FD16ppc scheme, and (c) Fourier spectral methods for azimuthal derivatives; (d) analytical solution. The contours of fluctuating pressure are for levels of $[1.75, 3.5, 7, 14] \times 10^{-6}$.

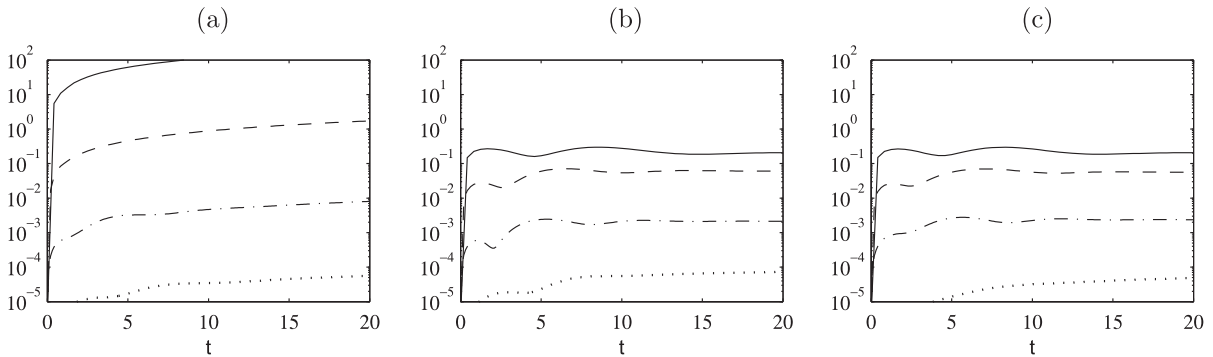


Fig. 6. Time variations of error \mathcal{E}_{sol} obtained with respect to the analytical solution for: — $PPC = 8$, --- $PPC = 16$, - · - · $PPC = 32$, and · · · · $PPC = 64$, using (a) 8th-order finite differences, (b) the FD8ppc, FD16ppc, FD32ppc, FD64ppc schemes (from top to bottom), and (c) Fourier spectral methods for azimuthal derivatives.

Table 2

Error \mathcal{E}_{sol} estimated at $t = 20$ with respect to the analytical solution for $PPC = 8, 16, 32,$ and 64 , using the FD8ppc, FD16ppc, FD32ppc, FD64ppc schemes (second column, from top to bottom), standard finite differences of order 4 (FDo4), 6 (FDo6), 8 (FDo8), 10 (FDo10) and 12 (FDo12), and Fourier spectral methods for azimuthal derivatives.

	Present schemes	FDo4	FDo6	FDo8	FDo10	FDo12	Fourier
PPC = 8	0.21	1050	480	220	100	47	0.21
PPC = 16	0.060	96	13	1.7	0.24	0.061	0.056
PPC = 32	4.0×10^{-3}	6.4	0.22	8.6×10^{-3}	2.1×10^{-3}	2.2×10^{-3}	2.4×10^{-3}
PPC = 64	1.1×10^{-4}	0.40	3.6×10^{-3}	0.9×10^{-4}	0.5×10^{-4}	0.5×10^{-4}	0.5×10^{-4}

Finally the errors \mathcal{E}_{sol} estimated at $t = 20$ for varying discretizations and differentiation operators in the azimuthal direction are collected in Table 2. They support the previous findings: for the present test case, the schemes designed in the paper are more appropriate than corresponding standard schemes for $PPC \leq 32$, and they yield results whose accuracy is comparable to that obtained using spectral methods.

4. Reduction of effective azimuthal discretization near cylindrical origin

4.1. Presentation of the method

When cylindrical equations are advanced in time using explicit algorithms, the time step might be severely limited because of the fine azimuthal mesh spacing near the origin, which is classically $\Delta r \Delta \theta$ at radial distance $r = \Delta r$. To alleviate this constraint, it is proposed to compute the azimuthal derivatives near $r = 0$ not as usually using finite differences from the directly adjacent points as:

$$\frac{\partial^* F}{\partial \theta} = \frac{1}{\Delta \theta} \sum_{j=-n}^n a_j F(\theta + j \Delta \theta),$$

but from points separated by $\Delta \theta_{FD} = m \Delta \theta$ ($m > 1$ is an integer) as:

$$\frac{\partial^* F}{\partial \theta_{FD}} = \frac{1}{\Delta \theta_{FD}} \sum_{j=-n}^n a_j F(\theta + j \Delta \theta_{FD})$$

The effective azimuthal mesh spacing near the origin is then affected by the coarsening ratio $\Delta \theta_{FD} / \Delta \theta$, and becomes $\Delta r \Delta \theta_{FD}$, which reduces the effective azimuthal discretization to $PPC_{FD} = 2\pi / \Delta \theta_{FD}$.

As illustrations, the calculation of derivatives in the azimuthal direction of a polar grid using 2nd-order finite differences is represented in Fig. 7. In the standard way, in Fig. 7(a), the derivatives at angle θ are evaluated from solutions at $\theta \pm \Delta \theta$, yielding an azimuthal resolution of $2\pi / \Delta \theta$. In the proposed approach, in Fig. 7(b), the effective azimuthal resolution near $r = 0$ is for instance lowered to $\pi / \Delta \theta$ by computing the derivatives near the origin, at angle θ , from solutions at $\theta \pm 2\Delta \theta$.

In the present finite-difference-based method, the effective resolution is consequently reduced near the origin, in the same way as in the classical approach consisting in removing the highest Fourier modes when using spectral methods [11,15–19]. Note that the azimuthal derivatives must still be estimated at all points. No point is removed, which implies that the number of numerical operations is the same. The time step however increases as the effective mesh spacing, from $\Delta t = \alpha \Delta r \Delta \theta$ to $\Delta t = \alpha \Delta r \Delta \theta_{FD}$, where the coefficient α is determined from the stability properties of the time integration scheme. The time-step limitation due to the use of cylindrical coordinates is therefore relaxed. In the case presented in Fig. 7(b), the time step can for example be doubled because the minimum effective azimuthal mesh spacing becomes $2\Delta r \Delta \theta$ instead of $\Delta r \Delta \theta$.

In practice, the reduction of the effective azimuthal discretization can be applied in different ways, depending notably on the grid density. One possibility is to gradually decrease the effective resolution near the origin as in simulations using spectral methods [11,15–19]. In these works, the summations yielding the azimuthal derivatives in the Fourier space are truncated to eliminate the highest wave numbers in such a way that the effective resolution in θ is nearly constant with radial location.

Another possibility which is proposed here using finite differences is to implement a series of doublings of the effective azimuthal discretization with the radial distance. Consider for instance a uniform polar grid containing $n_\theta = 256$ points, located from $r = 0$ every Δr . To decrease the effective azimuthal resolution near the origin down to 8 points per circle, coarsening ratios $\Delta \theta_{FD} / \Delta \theta$ can be specified as in Table 3, from 2 at $r = 31\Delta r$ up to 32 at $r = \Delta r$. As reported in the table, this results in effective azimuthal mesh spacings equal or higher than $32\Delta r \Delta \theta$. In this way the time step could be 32 times larger than the time step that is reachable using standard azimuthal differentiation.

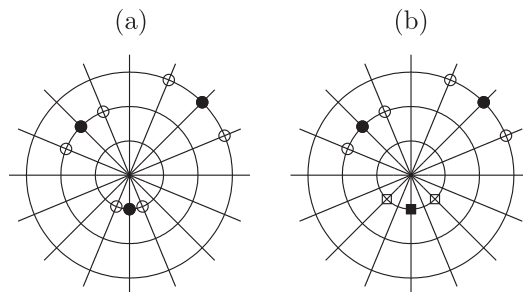


Fig. 7. Differentiation in the azimuthal direction on a polar grid, using 2nd-order finite differences: (a) standard method, and (b) reduced effective discretization near the origin. Derivatives at points ● and ■ are approximated from points ○ and □, respectively.

Table 3

Example of reduction of the effective azimuthal discretization near the origin on a $n_\theta = 256$ -point polar grid in which the first point is at $r = \Delta r$: coarsening ratio $\Delta\theta_{FD}/\Delta\theta$, and effective mesh spacing $r\Delta\theta_{FD}$ as a function of the radial distance.

$r/\Delta r$	$\Delta\theta_{FD}/\Delta\theta$	$r\Delta\theta_{FD}/\Delta r\Delta\theta$
1	32	32
2 → 3	16	32 → 48
4 → 7	8	32 → 56
8 → 15	4	32 → 60
16 → 31	2	32 → 62
32 → n_r	1	32 → n_r

4.2. Application to the propagation of an acoustic pulse

The method is applied to a two-dimensional propagation problem based on polar Euler Eq. (1). At $t = 0$, a Gaussian acoustic pulse placed in a mean flow of velocity $M = 0.5$ is specified from conditions (7) given in Section 3.3. The pulse is characterized by a magnitude $\mathcal{A} = 10^{-4}$ and a half-width $b = 3$, and is located at $x = -30$ and $y = 0$ on the left-hand side of origin 0. The acoustic wave generated by the pulse reaches point 0 at time $t = 20$. The problem is computed up to time $t = 40$, on a uniform polar grid containing $n_r = 81$ and $n_\theta = 256$ points in the radial and azimuthal directions. The radial mesh spacing is $\Delta r = 1$, and the first points near the origin are at $r = \Delta r/2$ following the method of Mohseni & Colonius [11]. In the radial direction, the derivatives are calculated using 14th-order finite differences.

In the azimuthal direction, six configurations with effective discretizations near the origin varying from $\text{PPC}_{FD} = n_\theta = 256$ down to $\text{PPC}_{FD} = n_\theta/32 = 8$ are first considered. Their acronyms and parameters are provided in Table 4. In the first simulation Pol_{256} , all azimuthal derivatives are evaluated classically using standard 10th-order finite-differences FD_{10} . In simulations Pol_{128} , Pol_{64} , Pol_{32} , Pol_{16} and Pol_8 , series of doublings of the effective azimuthal discretization are applied to obtain respectively $\text{PPC}_{FD} = 128, 64, 32, 16$ and 8 at the points placed at $r = \Delta r/2$, and minimum effective mesh spacings $r\Delta\theta_{FD} = \Delta r\Delta\theta, 2\Delta r\Delta\theta, 4\Delta r\Delta\theta, 8\Delta r\Delta\theta$ and $16\Delta r\Delta\theta$. The differentiation in the azimuthal direction is performed using FD_{10} for $\text{PPC}_{FD} = 256$ and 128 , but using the schemes designed in Section 3 for coarser effective discretizations, namely $\text{FD}_{64\text{ppc}}$ for $\text{PPC}_{FD} = 64$, $\text{FD}_{32\text{ppc}}$ for $\text{PPC}_{FD} = 32$, $\text{FD}_{16\text{ppc}}$ for $\text{PPC}_{FD} = 16$ and $\text{FD}_{8\text{ppc}}$ for $\text{PPC}_{FD} = 8$.

Time integration is performed using a low-storage 2nd-order 6-stage Runge–Kutta algorithm [24], and the time step is defined by $\Delta t = \text{CFL}\Delta r_{\min}(\Delta\theta_{FD})/(1 + M)$ with $\text{CFL} = 5/(2\pi) \simeq 0.8$. Computing up to time $t = 40$ consequently requires 3072 time steps in Pol_{256} , 1536 in Pol_{128} , 768 in Pol_{64} , 384 in Pol_{32} , 192 in Pol_{16} and 96 in Pol_8 .

In Pol_{256} , the flow variables are filtered explicitly at every 32nd iteration using a 14th-order filter in the radial direction and a 6th-order 11-point filter [33] in the azimuthal direction, sequentially, with a strength equal to unity. The same filterings are implemented in the other simulations, but at every 16th iteration in Pol_{128} , every 8th iteration in Pol_{64} , every 4th

Table 4

Parameters in Pol_{256} , Pol_{128} , Pol_{64} , Pol_{32} , Pol_{16} and Pol_8 with effective azimuthal discretizations of 256, 128, 64, 32, 16 and 8 points per circle near the origin: coarsening ratio $\Delta\theta_{FD}/\Delta\theta$, effective azimuthal discretization PPC_{FD} , effective azimuthal mesh spacing $r\Delta\theta_{FD}$, and schemes used for azimuthal differentiation, as a function of the radial distance.

Simulation	$r/\Delta r$	$\Delta\theta_{FD}/\Delta\theta$	PPC_{FD}	$r\Delta\theta_{FD}/\Delta r\Delta\theta$	schemes
Pol_{256}	$1/2 \rightarrow n_r - 1/2$	1	256	$1/2 \rightarrow n_r - 1/2$	FD_{10}
Pol_{128}	$1/2$	2	128	1	FD_{10}
	$3/2 \rightarrow n_r - 1/2$	1	256	$3/2 \rightarrow n_r - 1/2$	FD_{10}
Pol_{64}	$1/2$	4	64	2	$\text{FD}_{64\text{ppc}}$
	$3/2$	2	128	3	FD_{10}
	$5/2 \rightarrow n_r - 1/2$	1	256	$5/2 \rightarrow n_r - 1/2$	FD_{10}
Pol_{32}	$1/2$	8	32	4	$\text{FD}_{32\text{ppc}}$
	$3/2$	4	64	6	$\text{FD}_{64\text{ppc}}$
	$5/2 \rightarrow 7/2$	2	128	$5 \rightarrow 7$	FD_{10}
	$9/2 \rightarrow n_r - 1/2$	1	256	$9/2 \rightarrow n_r - 1/2$	FD_{10}
Pol_{16}	$1/2$	16	16	8	$\text{FD}_{16\text{ppc}}$
	$3/2$	8	32	12	$\text{FD}_{32\text{ppc}}$
	$5/2 \rightarrow 7/2$	4	64	$10 \rightarrow 14$	$\text{FD}_{64\text{ppc}}$
	$9/2 \rightarrow 15/2$	2	128	$9 \rightarrow 15$	FD_{10}
	$17/2 \rightarrow n_r - 1/2$	1	256	$17/2 \rightarrow n_r - 1/2$	FD_{10}
Pol_8	$1/2$	32	8	16	$\text{FD}_{8\text{ppc}}$
	$3/2$	16	16	24	$\text{FD}_{16\text{ppc}}$
	$5/2 \rightarrow 7/2$	8	32	$20 \rightarrow 28$	$\text{FD}_{32\text{ppc}}$
	$9/2 \rightarrow 15/2$	4	64	$18 \rightarrow 30$	$\text{FD}_{64\text{ppc}}$
	$17/2 \rightarrow 31/2$	2	128	$17 \rightarrow 31$	FD_{10}
	$33/2 \rightarrow n_r - 1/2$	1	256	$33/2 \rightarrow n_r - 1/2$	FD_{10}

iteration in Pol₃₂, every 2nd iteration in Pol₁₆ and every iteration in Pol₈, leading to a filtering frequency independent of the time step. For reduced resolutions, variables are filtered supplementally in the azimuthal direction, by applying the 11-point filter at strength and frequency defined above, to grid points separated by doubling distances from 2Δθ up to Δθ_{FD}, that is up to the effective azimuthal discretization. For PPC_{FD} = 64 for instance, filtering is performed three times in the azimuthal direction, for 256, then for 128 and finally for 64 points per circle. In this way the calculations of the derivatives and the variable filterings are carried out at same effective azimuthal resolution.

To discuss the quality of results, two additional computations are performed using spectral methods based on discrete Fourier transforms to evaluate the azimuthal derivatives [16]. They are referred to as Spec₂₅₆ and Spec₈ in Table 5, because their effective azimuthal discretizations near the origin are respectively of 256 and 8 points per circle. To achieve this, the summations used to compute the azimuthal derivatives in the Fourier space are fully considered in Spec₂₅₆, but truncated in Spec₈ so as to obtain a constant effective azimuthal mesh spacing of 16ΔrΔθ for r ≤ 31Δr/2 as reported in Table 5. Except for the azimuthal differentiation, simulations Spec₂₅₆ and Spec₈ are respectively identical to Pol₂₅₆ and Pol₈, implying same parameters for the grid, time integration, radial discretization, and azimuthal filtering. In particular, 3072 time steps are required in Spec₂₅₆, but only 96 in Pol₈.

The solutions obtained at t = 40 from the four simulations with coarser effective discretizations near the origin, namely Pol₃₂, Pol₁₆, Pol₈ and Spec₈, are represented in Fig. 8. Changes with the effective resolution near r = 0 are only clearly visible for Pol₈. For this simulation with PPC_{FD} = 8 at r = Δr/2, the inner contour of pressure displays small oscillations, which is not the case for Spec₈ for instance. They may be generated by the doublings of the effective discretization near the origin.

The differences found at t = 40 between the solutions from Pol₃₂, Pol₁₆, Pol₈ and Spec₈, and analytical solution (8) are displayed in Fig. 9. In all cases numerical errors are observed all around the acoustic wave propagating from the initial pulse. They appear higher with lower effective discretization near the origin, especially in Pol₈ and in Spec₈.

To quantify this, the error rates \mathcal{E}_{sol} between the computed and analytical solutions are determined from expression (9). Their time variations are presented in Fig. 10. They collapse very well in the simulations Pol₂₅₆, Pol₁₂₈, Pol₆₄, Pol₃₂, and Spec₂₅₆, with effective azimuthal discretizations equal or higher than 32 near the origin. In these cases, the errors resulting from the reduction of the effective azimuthal discretization are consequently lower than those from the other numerical tools. They appear however higher for coarser effective resolutions near the origin. The error rates \mathcal{E}_{sol} indeed increase slightly in Pol₁₆, and more significantly in Pol₈ and in Spec₈. A hump is in particular found around time t = 20 in Pol₈ when the acoustic wave is travelling around r = 0. It is certainly due to the generation of short-wave oscillations observed in Fig. 8(c), but it is progressively damped as selective filtering is applied to the flow variables. As a result, one gets similar errors at t = 40 in the two simulations Pol₈ and Spec₈ with an effective resolution of 8 points per circle near the origin, using finite differences or Fourier spectral methods for azimuthal differentiation. For completeness, it can be noted that the errors in Pol₈ have been checked not to vary appreciably with the time step, which supports that the errors are mainly related to the spatial discretization.

Table 5
Parameters in Spec₂₅₆ and Spec₈ using Fourier spectral methods for azimuthal differentiation with effective azimuthal discretizations of 256 and 8 points per circle near the origin: effective azimuthal mesh spacing $r\Delta\theta_{Fo}$.

Simulation	$r/\Delta r$	$r\Delta\theta_{Fo}/\Delta r\Delta\theta$
Spec ₂₅₆	1/2 → $n_r - 1/2$	1/2 → $n_r - 1/2$
Spec ₈	1/2 → 31/2 33/2 → $n_r - 1/2$	16 33/2 → $n_r - 1/2$

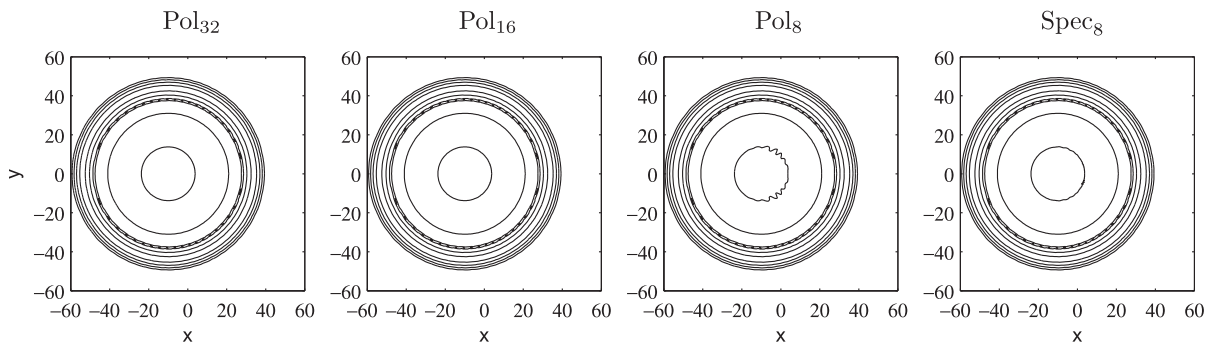


Fig. 8. Solutions obtained at time t = 40 from simulations Pol₃₂, Pol₁₆, Pol₈ and Spec₈. The contours of fluctuating pressure are for levels of $[0.03125, 0.125, 0.5, 2, 8] \times 10^{-6}$.

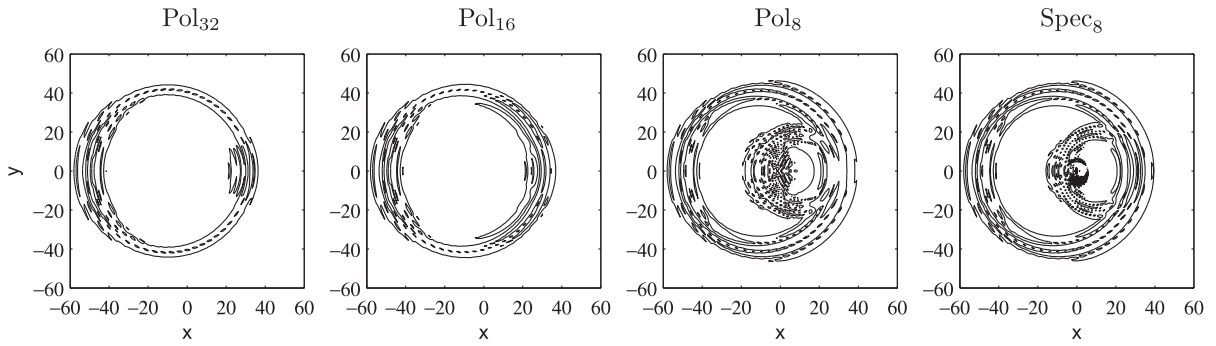


Fig. 9. Absolute value of the difference between the analytical solution and the solutions obtained at time $t = 40$ from simulations Pol₃₂, Pol₁₆, Pol₈ and Spec₈. The contours are for pressure levels of $[0.125, 0.5, 2] \times 10^{-8}$.

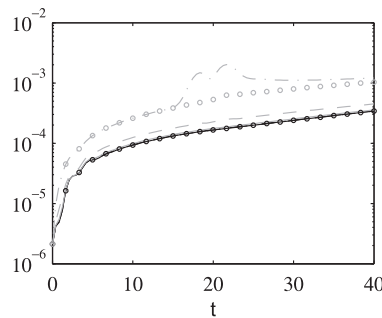


Fig. 10. Time variations of error ϵ_{sol} obtained with respect to the analytical solution for: — Pol₂₅₆, - - - Pol₁₂₈, - · - · Pol₆₄, — Pol₃₂, - - - Pol₁₆, - · - · Pol₈, ○ ○ ○ Spec₂₅₆, ○ ○ ○ Spec₈.

To evaluate the artefacts resulting from the changes in the azimuthal differentiation alone, comparisons are performed with the solution from Pol₂₅₆. They are shown in Fig. 11 for Pol₃₂, Pol₁₆, Pol₈ and Spec₈ at time $t = 40$. As expected, the discrepancies are of higher amplitude with lower effective resolution near the origin. Remarks can also be made regarding the error footprints. Errors are first observed in all simulations on an arc following the position of the circular acoustic wave generated by the initial pulse, with a maximum in the direction downstream of the origin. Additional errors, indicated by an inner round wave, are then found in the two simulations Pol₈ and Spec₈, when the effective discretization near $r = 0$ is 8 points per circle.

The error rates with respect to the solution p_{256} obtained from Pol₂₅₆ are finally determined as:

$$\epsilon_{256}(t) = \frac{[\int \int_S (p(t) - p_{256}(t))^2 dS]^{1/2}}{[\int \int_S (p(t=0) - 1/\gamma)^2 dS]^{1/2}}. \tag{10}$$

They are presented in Fig. 12 for the different simulations. They increase in time to reach at $t = 40$ values ranging from $\epsilon_{256} \simeq 3 \times 10^{-6}$ in Pol₁₂₈ up to $\epsilon_{256} \simeq 10^{-3}$ in Pol₈. The errors coming from the present approach therefore appear negligible

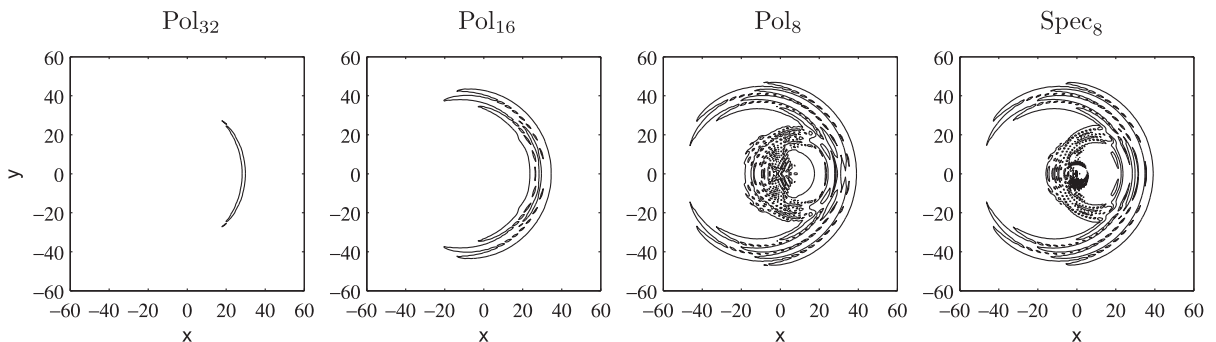


Fig. 11. Absolute value of the difference between the solution obtained at time $t = 40$ from simulation Pol₂₅₆, and those from Pol₃₂, Pol₁₆, Pol₈ and Spec₈. The contours are for pressure levels of $[0.125, 0.5, 2] \times 10^{-8}$.

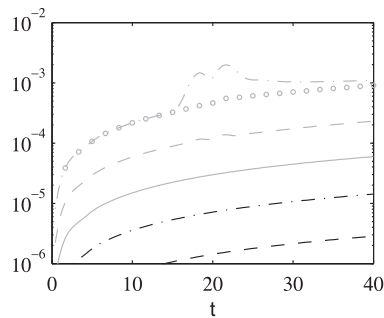


Fig. 12. Time variations of error \mathcal{E}_{256} obtained with respect to the solution from simulation Pol_{256} , for: --- Pol_{128} , - · - Pol_{64} , — Pol_{32} , - - - Pol_{16} , - · - Pol_8 , ○ ○ Spec_8 .

for large PPC_{FD} near the origin, and remain small for coarse effective resolution, in particular thanks to the schemes developed in Section 3. It is interesting to emphasize that the accuracy is still acceptable in Pol_8 . The tremendous increase of the time step, and the saving in computational cost in this simulation with $\text{PPC}_{FD} = 8$, are thus achieved without significantly deteriorating the numerical solution. The loss of accuracy is even found to be comparable to that observed in Spec_8 , in which the reduction of the effective azimuthal resolution down to 8 points per circle is performed using Fourier spectral methods.

5. Conclusion

In the present paper, an analysis of the errors that arise when the flow equations are solved in cylindrical coordinates using finite differences is presented. It shows that strong numerical artefacts might be generated by the computation of derivatives in the azimuthal direction. Centered 7-point or 9-point explicit finite differences are therefore derived specially for azimuthal differentiation. For an acoustic propagation problem, they provided results supporting that they enable to reach reasonable accuracy even for very coarse discretization. For 16 points per circle, the error rate is for instance only around 6% for the test case considered. To get comparable error rate using standard schemes, 12th-order finite differences based on a stencil of twice width are required. For 8 points per circle, the error rate is even about 200 times lower than the one obtained using 12th-order schemes.

An approach is then proposed to alleviate the time-step restriction due to the fine mesh spacing near the cylindrical origin when time integration is explicit. It consists in decreasing the effective azimuthal resolution at smaller radial location, as usually done using spectral methods, by implementing finite-difference stencils of larger azimuthal span. Using the schemes previously developed, good accuracy is found for an acoustic propagation problem, down to an effective azimuthal resolution of 8 points per circle near $r = 0$. In the latter case, for a cylindrical grid containing $n_\theta = 256$ points, the simulation is performed using a time step 32 times larger than in the simulation without reduction of the effective azimuthal discretization. The error rate is checked to be only around 0.1%, indicating that the accuracy of the solution is not significantly affected by the present approach.

The finite-difference-based methods presented in the paper are fast and easy to implement. Moreover, when applied to linear propagation problems using the 2D Euler equations, they yield solutions whose accuracy is similar to that achieved using Fourier spectral methods in the azimuthal direction. To examine their behaviours for more complicated flow configurations, additional work would naturally be necessary. It must however be noted that the methods have already been successfully employed in large-eddy simulations of turbulent round jets [21–23] solving the 3D cylindrical compressible Navier–Stokes equations.

Acknowledgments

The second author is grateful to the Centre National d'Etudes Spatiales (CNES) for financial support. This work was granted access to the French HPC resources of IDRIS under the allocation 2009-020204 made by GENCI (Grand Equipement National de Calcul Intensif).

References

- [1] S.A. Orszag, Fourier series on spheres, *Mon. Weather Rev.* 102 (1974) 56–75.
- [2] C. Canuto, M. Hussaini, A. Quarteroni, T. Zang, *Spectral Methods in Fluid Dynamics*, Springer Verlag, Berlin and New York, 1988.
- [3] J.P. Boyd, *Chebyshev and Fourier Spectral Methods*, second ed., Dover, New York, 2001.
- [4] W. Huang, D.M. Sloan, Pole condition for singular problems: the pseudospectral approximation, *J. Comput. Phys.* 107 (1993) 254–261.
- [5] T. Matsushima, P.S. Marcus, A spectral method for polar coordinates, *J. Comput. Phys.* 120 (2) (1995) 365–374.
- [6] G.S. Constantinescu, S.K. Lele, A highly accurate technique for the treatment of flow equations at the polar axis in cylindrical coordinates using series expansions, *J. Comput. Phys.* 183 (2002) 165–186.

- [7] F. Domenichini, B. Baccani, A formulation of Navier–Stokes problem in cylindrical coordinates applied to the 3D entry jet in a duct, *J. Comput. Phys.* (2004) 177–191.
- [8] M. Vinokur, Conservation equations of gasdynamics in curvilinear coordinate systems, *J. Comput. Phys.* 14 (1974) 105–125.
- [9] R. Verzicco, P. Orlandi, A finite-difference scheme for three-dimensional incompressible flows in cylindrical coordinates, *J. Comput. Phys.* 123 (1996) 402–414.
- [10] B.E. Mitchell, S.K. Lele, P. Moin, Direct computation of the sound generated by vortex pairing in an axisymmetric jet, *J. Fluid Mech.* 383 (1999) 113–142.
- [11] K. Mohseni, T. Colonius, Numerical treatment of polar coordinate singularities, *J. Comput. Phys.* 157 (2) (2000) 787–795.
- [12] Y. Kurihara, Numerical integration of the primitive equations on a spherical grid, *Mon. Weather Rev.* 93 (7) (1965) 399–415.
- [13] J.G.M. Eggels, F. Unger, M.H. Weiss, J. Westerweel, R.J. Adrian, R. Friedrich, F.T.M. Nieustadt, Fully developed turbulent pipe flow: a comparison between direct numerical simulation and experiment, *J. Fluid Mech.* 26 (1994) 175–209.
- [14] K. Akselvoll, P. Moin, An efficient method for temporal integration of the Navier–Stokes equations in confined axisymmetric geometries, *J. Comput. Phys.* 125 (1996) 454–463.
- [15] B. Fornberg, A pseudospectral approach for polar and spherical geometries, *SIAM J. Sci. Comput.* 16 (5) (1995) 1071–1081.
- [16] J.B. Freund, P. Moin, S.K. Lele, *Compressibility Effects in a Turbulent Annular Mixing Layer*, TF-72 Stanford University, 1997.
- [17] J.B. Freund, S.K. Lele, P. Moin, Numerical simulation of a Mach 1.92 turbulent jet and its sound field, *AIAA J.* 38 (11) (2000) 2023–2031.
- [18] C. Gissinger, A. Iskakov, S. Fauve, E. Dormy, Effect of magnetic boundary conditions on the dynamo threshold of von Kármán swirling flows, *Euro. Phys. Lett.* 82 (2008) 29001.
- [19] F. Keiderling, L. Kleiser, C. Bogey, Numerical study of eigenmode forcing effects on jet flow development and noise generation mechanisms, *Phys. Fluids* 21 (2009) 045106.
- [20] K. Fukagata, N. Kasagi, Highly energy-conservative finite difference method for the cylindrical coordinate system, *J. Comput. Phys.* 181 (2002) 478–498.
- [21] C. Bogey, O. Marsden, C. Bailly, Large-Eddy simulation of the flow and acoustic fields of a Reynolds number 10^5 subsonic jet with tripped exit boundary layers, *Phys. Fluids* (2010), see also AIAA-2010-3727, 2010. Submitted for publication.
- [22] C. Bogey, C. Bailly, Influence of nozzle-exit boundary-layer conditions on the flow and acoustic fields of initially laminar jets, *J. Fluid Mech.* 663 (2010) 507–538.
- [23] N. de Cacqueray, C. Bogey, C. Bailly, Direct noise computation of a shocked and heated jet at a Mach number of 3.30, AIAA-2010-3732, 2010.
- [24] C. Bogey, C. Bailly, A family of low dispersive and low dissipative explicit schemes for flow and noise computations, *J. Comput. Phys.* 194 (1) (2004) 194–214.
- [25] C.K.W. Tam, J.C. Webb, Dispersion-relation-preserving finite difference schemes for computational acoustics, *J. Comput. Phys.* 107 (1993) 262–281.
- [26] C.K.W. Tam, Benchmark problems and solutions, in: *ICASE/LaRC Workshop on Benchmark Problems in Computational Aeroacoustics*, NASA CP 3300, 1995, pp. 1–13.
- [27] S.K. Lele, Compact finite difference schemes with spectral-like resolution, *J. Comput. Phys.* 103 (1) (1992) 16–42.
- [28] C.K.W. Tam, Computational aeroacoustics: issues and methods, *AIAA J.* 33 (10) (1995) 1788–1796.
- [29] M.R. Visbal, D.V. Gaitonde, High-order-accurate methods for complex unsteady subsonic flows, *AIAA J.* 37 (10) (1999) 1231–1239.
- [30] C. Bogey, C. Bailly, On the application of explicit filtering to the variables or fluxes of linear equations, *J. Comput. Phys.* 225 (2007) 1211–1217.
- [31] C.K.W. Tam, Z. Dong, Radiation and outflow boundary conditions for direct computation of acoustic and flow disturbances in a nonuniform mean flow, *J. Comput. Acoust.* 4 (2) (1996) 175–201.
- [32] J. Berland, C. Bogey, O. Marsden, C. Bailly, High-order, low dispersive and low dissipative explicit schemes for multi-scale and boundary problems, *J. Comput. Phys.* 224 (2) (2007) 637–662.
- [33] C. Bogey, N. de Cacqueray, C. Bailly, A shock-capturing methodology based on adaptive spatial filtering for high-order non-linear computations, *J. Comput. Phys.* 228 (5) (2009) 1447–1465.